Lightning Phenomenology Notes

Note 16

July 1985

LIGHTNING RETURN STROKE-A NUMERICAL SIMULATION INCLUDING A MULTIGROUP RADIATIVE TRANSPORT ALGORITHM

A. H. PAXTON

R.L. GARDNER

L. BAKER

Mission Research Corporation

1720 Randolph Road, S.E.

Albuquerque, New Mexico 87106

Abstract

A numerical model that includes a multigroup radiative transport treatment was used to calculate the optical radiance corresponding to an assumed current waveform. The calculation compares well with the experimental data that are available.

The time development of the temperature, pressure, density, and electrical conductivity profiles across the channel were investigated, as was the energy balance for the process.

CONTENTS

I. INTRODUCTION

Recently, measurements of the optical radiance of lightning return stroke channels have been described.[1] It is therefore of interest both for theoretical and practical reasons to develop the capability to estimate the electrical current waveform from the optical signature of a return stroke. We have used a numerical model for a return stroke channel to obtain the optical radiance corresponding to an electrical current waveform.

Our numerical model consists of a multigroup radiative transport treatment combined with a lightning channel model which is otherwise very similar to that applied by Plooster.[2] The hydrodynamics treatment is described in Section II of this paper. The radiative transport algorithm is discussed in Section III, and our calculated results are presented in Section IV and compared with the experimental data of Guo and Krider.[1] In contrast to other recent work [3,4], no effort is made to calculate the time dependence of the current; a waveform is specified prior to the calculation. The current is assumed to exist in an axially symmetric channel so the calculation is one dimensional, treating a single slice throught the channel.

II. HYDRODYNAMICS TREATMENT

A computer code described in Gardner's dissertation[5] was modified for this study. The model is based in large part on one developed by Plooster in a series of papers[2,6-8] for long sparks and natural lightning. The model used in this study differs primarily in the radiation treatment.

The model is one-dimensional in cylindrical coordinates. It allows gas heating by a predetermined current and calculates the electrical conductivity of the gas. A complex equation of state, which allows molecules, neutral atoms, and once and twice ionized atomic species is included. Cooling by expansion and radiation is modeled and shocks are treated using a frequency pressure term.[9]

The hydrodynamic equations are based on a well-known treatment by Richtmyer and Morton[9] and are in Lagrangian form. The choice of Lagrangian coordinate which gives the initial position of each mass point relative to a uniform mass density is

$$R^2 = \frac{2}{\rho_0} \int_0^r \rho(r) r dr \tag{1}$$

The differential equations to be solved are

$$\frac{\partial R}{\partial t} = u$$

$$\frac{\partial u}{\partial t} = -\frac{1}{\rho_0} \frac{\partial (p + q)}{\partial r} \frac{R}{r}$$

$$\frac{\partial \varepsilon}{\partial t} = -(p + q) \frac{\partial V}{\partial t} + Q - S$$

$$V = \frac{1}{\rho_0} \frac{R}{r} \frac{\partial R}{\partial r}$$

$$p = p(n, V) \tag{2}$$

where Q is the power added by joule heating, S is the radiation power loss, and the pseudo-viscous pressure is

$$q = \frac{\ell^2}{V}\left(\frac{\partial u}{\partial r}\right)^2 \qquad \text{if} \quad \frac{\partial u}{\partial r} < 0$$

$$q = 0 \qquad \text{if} \quad \frac{\partial u}{\partial r} \geq 0 \tag{3}$$

where u is the velocity in the Lagrangian frame. V is the specific volume or $V = 1/\rho$ and r is the distance in the fixed cylindrical coordinates.

The pseudo-viscous pressure causes the spreading of the leading edge of the shock wave across several zones with the constant length scale ℓ determining the spread. These equations were solved by using finite difference techniques. Richtmyer and Morton[9] provide the following standard difference scheme to determine the variables at the n+1st time step from their values at the nth time step. The j index labels fixed mass elements according to their initial uniform grid spacing in r. The difference equations are

$$\frac{R_j^{n+1} - R_j^n}{\Delta t} = u_j^{n+1} \tag{4}$$

$$\frac{u_j^{n+1} - u_j^n}{\Delta t} = -\frac{1}{\rho_0}\frac{(\delta p)_j^n + (\delta q)_j^n}{\Delta r}\left(\frac{R_j^n}{r_j}\right) \tag{5}$$

$$V_{j+1/2}^{n+1} = \frac{1}{\rho_0}\frac{\left(R_{j+1}^{n+1}\right)^2 - \left(R_j^{n+1}\right)^2}{r_{j+1}^2 - r_j^2} \tag{6}$$

$$\varepsilon_{j+1/2}^{n+1} - \varepsilon_{j+1/2}^{n} + \left(\frac{p_{j+1/2}^{n+1} + p_{j+1/2}^{n}}{2} + q_{j+1/2}^{n}\right) \times \left(V_{j+1/2}^{n+1} - V_{j+1/2}^{n}\right) = Q_{j+1/2}^{n} - S_{j+1/2}^{n} \tag{7}$$

$$p_{j+1/2}^{n+1} = \frac{(\gamma - 1)\, n_{j+1/2}^{n+1}}{V_{j+1/2}^{n+1}} \tag{8}$$

$$q^n_{j+1/2} = \frac{2\alpha^2}{V^n_{j+1/2} + V^{n-1}_{j+1/2}} \left[(\delta u)^n_{j+1/2}\right]^2 \quad \text{if} \quad (\delta u)^n_{j+1/2} < 0 \tag{9}$$

$$q^n_{j+1/2} = 0 \quad \text{if} \quad (\delta u)^n_{j+1/2} \geq 0$$

where $\ell = \alpha \Delta r$.

The pressures p and q, specific volume V and internal energy density η are defined at each grid midpoint. The constant α determining the spread of the shock, was set equal to 2 in these calculations. This value has the effect of spreading the shock over about 5-6 radial zones out of 128 total radial z nes. To maintain stability limits were placed on the time step, Δt (Refs. 10, 14), so that the usual Courant condition was satisfied. That is, the time step was no larger than the time required for a wave to cross a radial zone at the adiabatic sound speed, v. The pseudo-viscous term also places a limit on the time step. For α defined as in in Equation 9 the limit is

$$\Delta t < \frac{1}{4\alpha^2} \frac{R_{j+1} - R_j}{u_{j+1} - u_j} \tag{10}$$

Following Plooster[4] the time step was chosen to be 0.75 of the minimum of the limits obtained using Equation 10 and the Courant condition. A smooth initial temperature distribution, T(r), was used,

$$T(r) = T_0 + \frac{T_{max}}{\left(1 + \frac{r^2}{\alpha_0^2}\right)^2} \tag{11}$$

A uniform initial density was used in our calculations.

1. EQUATION OF STATE

We used an approximate equation of state for air that was developed by Plooster for spark and lightning calculations. Populations of molecules, atoms, singly ionized, and doubly ionized species were calculated using the Saha equation. Dissociation and ionization energies were computed from weighted averages of the values for nitrogen and oxygen. Plooster's equation of state is described in References 6 and 7.

In deriving the equation of state, it was assumed that the reactions take place serially, that is, all molecules are completely dissociated before ionization begins and all dissociated molecules are ionized once before second ionization begins. This technique allows two-species solution of each Saha equation rather than simultaneous solution for all species.

It was also assumed that the electrons are in local thermal equilibrium with the heavy particles. In a large electric field, the temperature of the electrons in a plasma exceeds the temperature of the heavy particles. An equation relating the electron temperature to the gas temperature and the electric field is.[10]

$$T_e^2 - T_g T_e = \left(\frac{m_g}{9m_e}\right)\left(\frac{e\lambda_e E}{K}\right)^2 \qquad (12)$$

where λ_e is the mean free path of the electrons m_g is the mass of a gas atom m_d is the mass of an electron, and E is the electric field. This expression was evaluated to obtain an estimate of $T_e - T_g$. The temperature difference was significant only at very early times. After

about a microsecond, equilibrium existed between the electrons and the heavy particles. Prior to this time, nonequilibrium effects may occur, but for the constant density initial conditions we assumed, our calculations never showed an electron temperature that exceeded the heavy particle temperature by more than 20 percent.

2. ELECTRICAL ENERGY INPUT

The electrical conductivity in $(S/m)^{-1}$ as a function of the radial coordinate is[9,10].

$$\sigma = \frac{4.173 \times 10^{-8} (A_1 + A_2) T^{-1/2}}{2 \times 10^{-15} (1 - A_1) + A_1 \langle a_i \rangle} \tag{13}$$

where A_1 and A_2 are the fractions of singly and doubly ionized atoms, and the average electron ion cross section is given by

$$\langle a_i \rangle = 2.8 \times 10^{-6} T^{-2} \left[(A_1 + 3A_2)/(A_1 + A_2) \right]^2 \times \left\{ \log \; 1.727 \times 10^{-5} \left[(A_1 + A_2)/(A_1 + 3A_2) \right] T \times (A_1 \rho)^{-1/3} \right\}$$

Each of the annular zones has a resistance per unit length calculated from Equation 13 and the area of the zone. The total current in the gas column is then apportioned to all of the annular zones as if they were an array of resistors connected in parallel. The diffusion time of the current into the conducting cylinder has been assumed to be short compared to a time step.

III. RADIATIVE TRANSPORT

A multigroup radiative transport algorithm using the diffusion approximation was included in the computer code to estimate the power of the optical radiation in the band of sensitivity of a detector used by Guo and Krider to measure the radiance per unit length of lightning channels.[1] A further aim was the improvement of the calculated energy input to the lightning channel. The radiant energy transfer between regions of the gas was improved, and the difference between results obtained by Plooster and the results presented here for the same case are attributable to this improvement.

The radiative transport algorithm used is described in detail in Reference 11. The spectrum of optical radiation was divided into frequency intervals called groups. The group boundaries were selected to minimize the opacity variation within each group. A single value of the opacity was assigned to each group, and the reciprocal mean was used. This type of average is more accurate for the optically thick case, in which the radiation is absorbed and reradiated a number of times in traversing the calculational grid, than for the optically thin case. In the limit in which groups are narrow enough to resolve the opacity versus frequency function, the algorithm used is valid in both the optically thick and optically thin limits.

The channel is optically thick in the far ultraviolet and is optically thin in the visible and infrared. Therefore, the far ultraviolet radiation has the effect of enlarging the channel, while only radiation in the near

ultraviolet, visible, and infrared causes energy loss. Ultraviolet radiation is the dominant mechanism of energy transfer from the hot conducting gas to the cooler gas in the outer part of the channel, and thermal conduction by the gas was not treated in the calculated results.

The diffusion approximation is also known as the P_1 method, which refers to the first-order expansion of the intensity in spherical harmonics. With the Marshak boundary condition, which we used, this approximation gives radiant energy densities that are accurate in the optically thick limit, but the energy densities are overestimated in the optically thin limit. However, the power radiated by the hot part of the channel is almost independent of the radiant energy density for optically thin bands, and the energy in thin bands that is reabsorbed in the cooler gas is a negligible fraction of the energy radiated in the hot region. Therefore, large errors would result if the calculated output flux at the edge of the grid had been used to obtain the radiated power in the band of interest, but by summing the net radiated power over all grid zones, accurate results were obtained.

1. RADIATIVE TRANSPORT ALGORITHM

The radiant field is completely specified by the intensity function, $I(t,\vec{r},\vec{\alpha},\nu)$, where t is the time, $\vec{r}$ is the location, $\vec{\alpha}$ is a unit vector in the direction of travel, and ν is the frequency. At a point interior to the lightning channel, the light that is radiated by the gas in a differential volume will travel away in all directions. Light also arrives at the point from all directions, and any ray that passes through the differential volume is partially absorbed. The intensity $I(t,\vec{r},\vec{\alpha},\nu)d\Omega d\nu$ is the flux with

frequency between ν and $\nu + d\nu$ within solid angle $d\Omega$ of a light ray with direction $\vec{\alpha}$ (see Fig. 1). The light ray passes through point $\vec{r}$. The intensity has units $W/(m^2\ sr\ Hz)$.

The equation of radiative transfer is

$$\dot{I} \equiv \left(\frac{\partial}{\partial t} + c\vec{\alpha} \cdot \nabla\right) I = \text{Sources} - \text{Sinks} \tag{14}$$

The convective derivative of the intensity function is the intensity created minus the intensity absorbed. The sinks are

$$\text{Sinks} = c(k_{abs} + k_{scat})\, I \tag{15}$$

The intensity loss due to scattering from one frequency to another is included in k_{scat}. The frequency- and temperature-dependent absorption coefficient per unit distance is k_{abs}. The source terms are

$$\text{Source} = ck_{abs}\ B(T,\nu) + S_{scat} \tag{16}$$

where

$$B(T,\nu) = \frac{2}{c^2} \frac{h\nu^3}{e^{h\nu/KT} - 1}$$

and S_{scat} is the intensity gain due to scattering from one frequency to another and $ck_{abs}\ B(T,\nu)$ is the emitted radiation. $B(T,\nu)$ is the Planck function for the blackbody intensity spectrum. The scattering terms are small compared to the absorptivities and may therefore be neglected.

Ignoring the scattering terms, Equation 14 becomes

$$\dot{I} \equiv \left(\frac{\partial}{\partial t} + c\vec{\alpha} \cdot \nabla\right) I = ck_{abs}\ (B(T,\nu) - I) \tag{17}$$

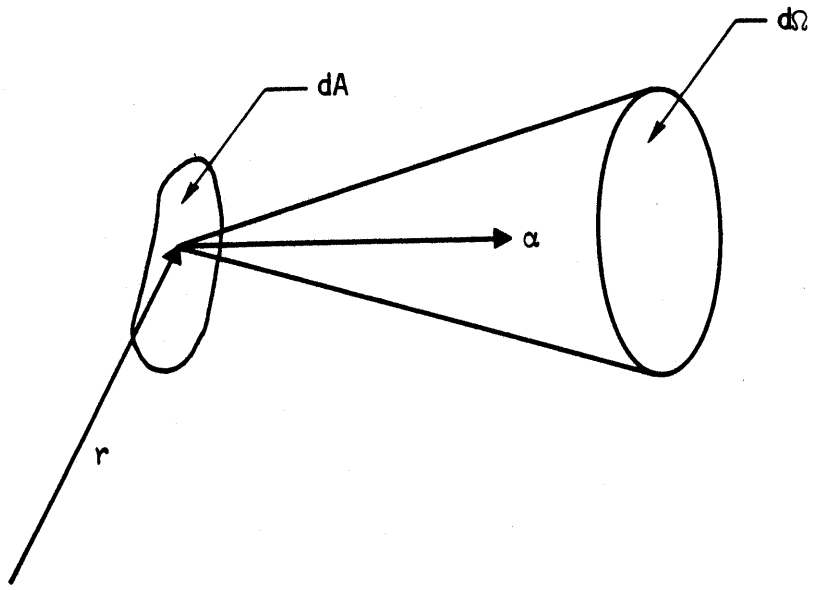

Figure 1. Illustration of the vectors and differential elements that specify the intensity function.

In the optically thick steady-state case in which absorption exactly cancels emission, $I = B(T,\nu)$. In the optically thin limit, $I \ll B(T,\nu)$ and the emission rate is simply

$$\dot{I} \simeq ck_{abs} \quad B(T,\nu) \tag{18}$$

This equation justifies our lack of concern for the accuracy of I for optically thin bands, provided that $I \ll B(T,\nu)$. Equation 17 was used to obtain the radiated power in each volume element rather than obtaining it from the outward component of I at the edge of the grid.

The diffusion approximation of Equation 17 is obtained in terms of the energy density of the radiation field, which is 1/c times the integral of I over 4π steradians, $U = 1/c \int I d\Omega$. By assuming that I is nearly isotropic, the diffusion approximation is obtained.[13]

$$\left(\frac{1}{c}\frac{\partial}{\partial t} - \nabla \cdot \frac{1}{3k} \nabla\right) U = k\left(\frac{4\pi}{c} \quad B(T,\nu) - U\right) \tag{19}$$

At the center of the coordinate system, the boundary condition $\partial U/\partial r = 0$ was applied. The boundary condition applied at the edge of the grid is a Marshack condition of the form

$$\frac{2}{3k}\frac{\partial U}{\partial r} + U = 0 \tag{20}$$

A standard tridiagonal finite-difference algorithm was used to solve Equation 19 numerically.[13]

Spectral lines have not been treated individually, but are included in the continuum absorptivities. Their contributions to the opacities are therefore somewhat overemphasized.[14,15]

Opacity tables of Reference 15 were used in the calculations.

Improved numerical stability of our code resulted when the central boundary condition, $\partial U/\partial r = 0$, was incorporated as a parabolic fit using the centered locations of the energy density values. The coordinate system that we used has $r_1 = 0$. The energy density U_1 is located at radius $r_2/2$, and U_2 is positioned at $(r_2 + r_3)/2$. The fields U_1 and U_2 are on a parabola that passes through some value U_0 at $r = 0$,

$$U_1 = ar_2^2/4 + U_0 \tag{21}$$

$$U_2 = a(r_2^2/4 + r_2r_3/2 + r_3^2/r) + U_0 \tag{22}$$

The value of a is then,

$$a = (U_2 - U_1)/(r_3^2/4 + r_2r_3/2) \tag{23}$$

And the derivative and second derivative of U at the first grid point are

$$\left.\frac{\partial U}{\partial r}\right|_{\frac{r_2}{2}} = ar_2 \tag{24}$$

and

$$\left.\frac{\partial^2 U}{\partial r^2}\right|_{\frac{r_2}{2}} = 2a \tag{25}$$

Equations 24 and 25 are substituted into the difference equation corresponding to Equation 19 to incorporate the boundary condition.

2. SIMULATED SPECTRAL TEMPERATURE

A common method of measuring the temperature of a hot gas is to measure the intensities of two spectral lines and compare them. The intensities of the lines are

$$I_{ij} = \frac{g_i}{U(T)} n(T) e^{-E_i/KT} A_{ij} h\nu_{ij} \tag{26}$$

where $n(T)$ is the atom or ion number density of the appropriate species, g_i is the degeneracy of state i, E_i is the energy of state i, A_{ij} is the Einstein coefficient, and $U(T)$ is the partition function of the atom or ion. The spectral temperature of a gas is determined by measuring the intensities of radiation from two transitions.

The ratio of the intensities is

$$\frac{I_{ij}}{I_{\ell k}} = \frac{g_i A_{ij} \nu_{ij} e^{-E_i/KT}}{g_\ell A_{\ell k} \nu_{\ell k} e^{-E_\ell/KT}} \tag{27}$$

and

$$T = \log\left[\left(\frac{I_{ij} g_\ell A_{\ell k} \nu_{\ell k}}{I_{\ell k} g_i A_{ij} \nu_{ij}}\right)\right]^{-1} \frac{E_\ell - E_i}{K} \tag{28}$$

This is an average weighted by n/U, which is a function of the temperature. For example, if one uses transitions of neutral atoms of nitrogen, the temperature will correspond to the cooler outer portion of the channel since ionization is nearly complete in the hotter region, where the number density of neutral atoms is very small. At temperatures of 20,000 K,

nitrogen is singly ionized, so transitions of N_{II} are appropriate to monitor the central region of the channel.

The same lines used by Plooster were applied to simulate the spectral temperature so that his calculations could be compared with this study. The $3s_1p^* - 3p\,^1D$ and $3d\,^3F^* - 4f\,^3G$ transitions of N_{II} were used. The ratio of the intensities was obtained using

$$\frac{\overline{I}_{ij}}{\overline{I}_{k\ell}} = \frac{g_i A_{ij} \nu_{ij} \int \frac{n}{U} e^{-E_i/KT} dr}{g_k A_{k\ell} \nu_{k\ell} \int \frac{n}{U} e^{-E_k/KT} dr} \qquad (29)$$

The partition function, U, was summed over 25 states of N_{II}. This includes all states with energy below $h\nu_m = 3.98 \times 10^{-11}$ Erg. At T = 40,000 K, $\exp(-h\nu_m/KT)$ is about 7×10^{-4}, so 25 states should suffice. The simulated spectral temperature is obtained by substituting $\overline{I}_{ij}/\overline{I}_{k\ell}$ from Equation 29 into Equation 28.

3. ESTIMATE OF THERMAL CONDUCTION AND CONVECTIVE COOLING

The behavior of a lightning channel is governed by a complicated set of energy gains and losses. The primary gain is by joule heating. Important losses are by optical radiation, ionization and expansion. Not treated in the present model are thermal conduction and convective cooling. Both experiments and theoretial calculations have been performed to determine the effect of convection on laboratory discharges.

Using the results of J. M. Picone, et al.[16] cooling times of about 400 s^{-1} are obtained along with an effective diffusion coefficient of

approximately 5 x 10^{-2} m^2/s. At a temperature of T = 3 eV and an electron number density of N = 2 x 10^{24} m^{-3}, the corresponding diffusion coefficient for electron thermal conduction is

$$K_e \sim \frac{1.3 \times 10^{23} \; T^{5/2}(eV)}{N \ell n \Lambda} = 0.5 \; m^2/s \qquad (30)$$

For radiative losses

$$K_R \simeq \frac{c}{3k_{abs}} \qquad (31)$$

which gives $K_R \simeq 1 \times 10^5$ m^2/s at 3 eV. Thus, radiative losses are orders of magnitude larger than convective cooling and electron thermal conduction effects, at least while the channel is fairly hot ($\gtrsim 10^4$ K) and moderately optically thick. As the channelexpands and cools, both radiative and convective losses will decrease, although the former will fall more rapidly.

IV. COMPARISON WITH EXPERIMENT

Natural lightning has been studied theoretically and a number of its properties have been determined experimentally. These results have provided a basis for the verification of our computer code. A test calculation using the code with a current pulse that peaks at a typical value of 20 kA for natural lightning is discussed. Comparison is made with Plooster's calculated results[2] by using a current pulse shape

$$I = \begin{cases} I_0 \, t/t_r \, , & t < t_r \\ I_0 \, e^{-(t-t_r)/t_d} \, , & t > t_r \end{cases} \qquad (32)$$

where the peak current $I_0 = 20$ kA; the rise time $t_r = 5 \times 10^{-6}$ s; the decay time $t_d = 5 \times 10^{-5}$ s.

As was described previously, this code uses the same hydrodynamics algorithm as Plooster did with the exception that in the code described here a boundary condition that will transmit a shock wave was introduced so that adequate resolution can be maintained at late times, while he used a grid doubling algorithm that always kept the shock wave within the grid boundary. We used the same grid throughout a calculation to avoid complications in treating the boundary conditions for the radiation energy density in the multigroup diffusion model of the radiative transport.

The most significant difference between our code and Plooster's is in the treatment of radiative transport. Plooster used a single temperature-independent opacity at all wavelengths to obtain a radiation loss for each grid point that varied as T^4. He separately treated a term that redistributed energy among grid points, again using a single temperature-independent opacity.

In contrast, this study uses the much more detailed radiative transport algorithm described earlier. It incorporates a table of temperature- and frequency-dependent opacities and uses the diffusion approximation to treat the transport. This detailed treatment was necessary to obtain an estimate

of the power radiated into a specific frequency range for comparison with experiment. The radiative energy loss and redistribution predicted using this model should be more accurate than Plooster's.

Temperature, pressure, density, and conductivity profiles were calculated for the current waveform described by Equation 32. The temperature profiles at five times are drawn in Figure 2, and the density profiles are shown in Figure 3. The calculation was begun with a very narrow channel with a peak temperature of about 8,000 K as shown in the temperature profile at 0.7 μs in Figure 2. The calculation was begun with a constant density gas that has begun to expand only within a fraction of a millimeter of the axis at 0.07 μs as shown on the density plot. At 4 μs the temperature has increased to 28,000 K and the hot channel has a radius of about 0.5 cm. As is shown in Figure 3, the material has expanded to create a very low density in the hot channel, and a high-density shock wave exists at its boundary. After this, the central temperature of the channel decreases as the channel expands with time. By the time 11 μs have passed, the shock wave has separated from the hot gas column and is passing through the cool air.

The pressure profiles are shown in Figure 4, with the shock wave traveling outward as time passes. The shock wave is shown passing through the grid boundary in Figure 5, which is plotted with a logarithmic scale. The dip at 4.7 cm in the curve with t = 91 μs is a reflection from the boundary of a small fraction of the leading edge of the pressure wave, as most of the wave passes through the transmissive boundary. This reflected wave is weak enough that it does not cause significant errors. The corresponding temperature profiles, also drawn with a logarithmic scale, are shown in Figure 6. The shock wave is traveling much faster than the hot channel is growing at these times.

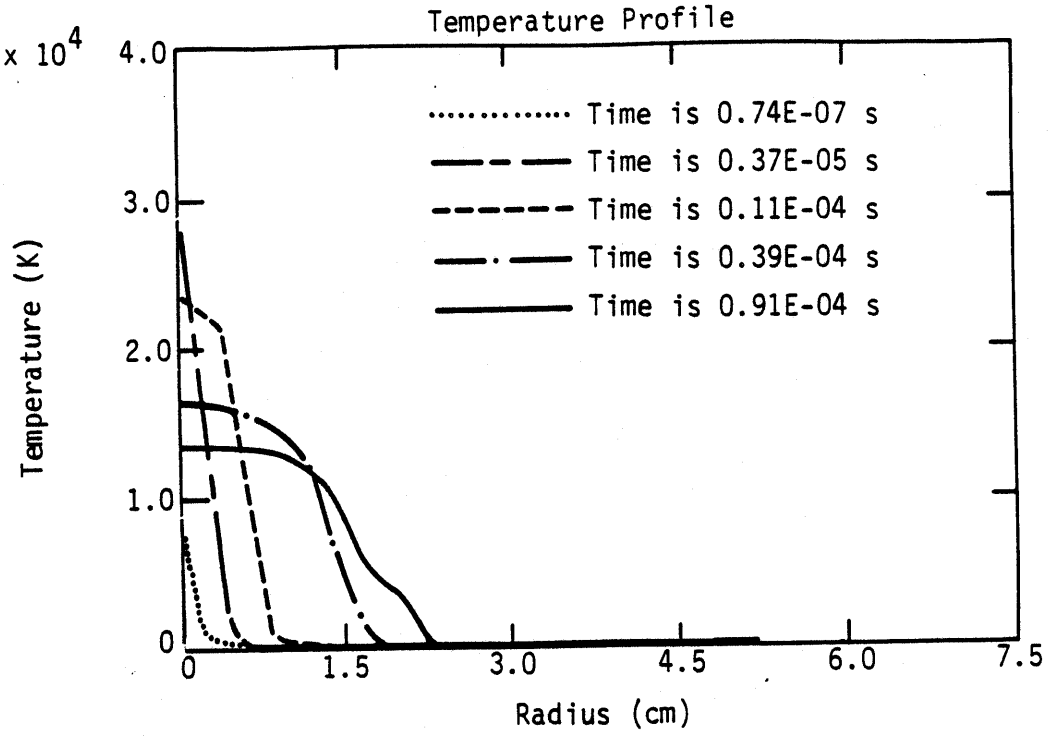

Figure 2. Simulated temperature profiles of a lightning return stroke channel at various timew with I_0 = 20 kA, t_r = 5 μs, and t_d = 50 μs.

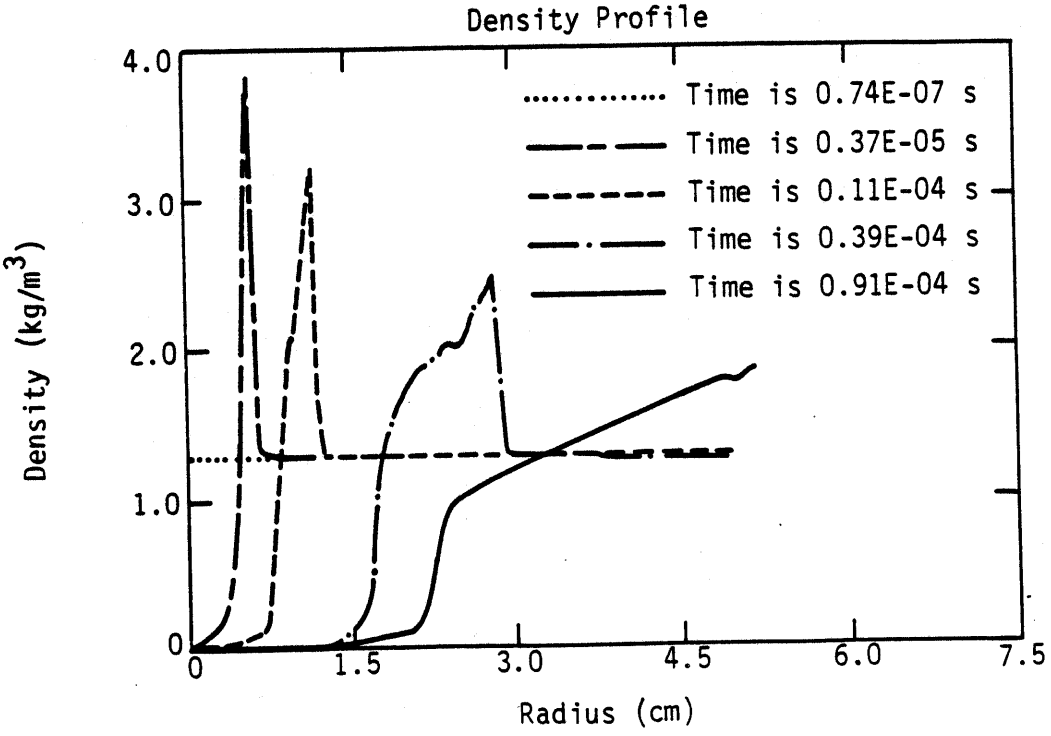

Figure 3. Density profiles of a lightning channel.

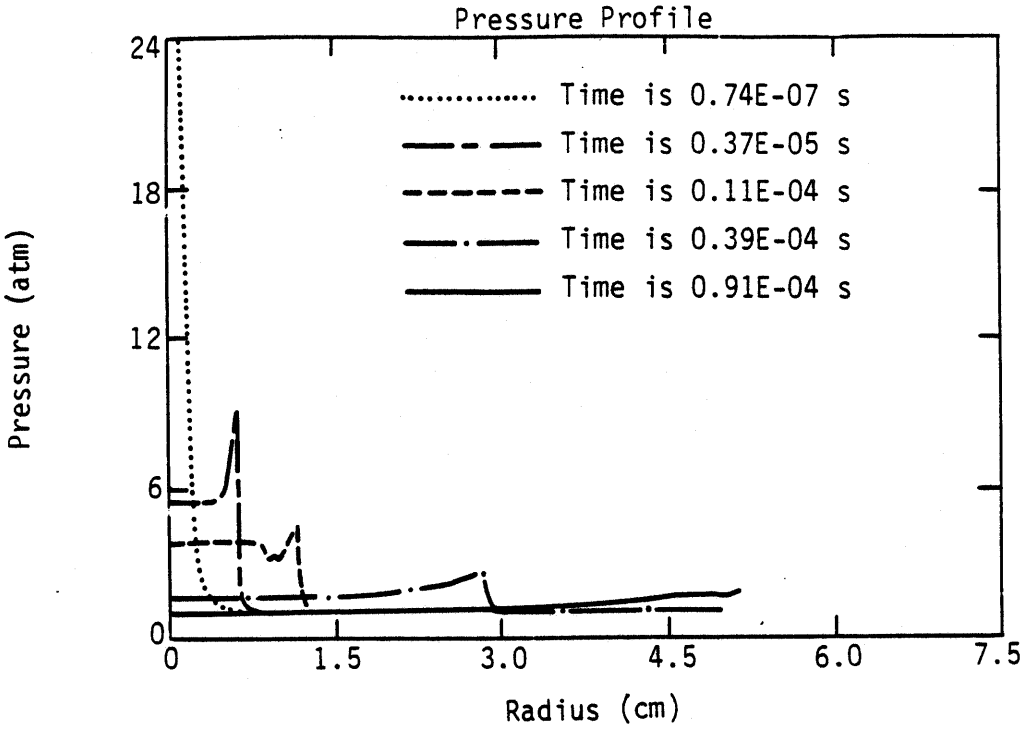

Figure 4. Pressure profiles of a lightning channel.

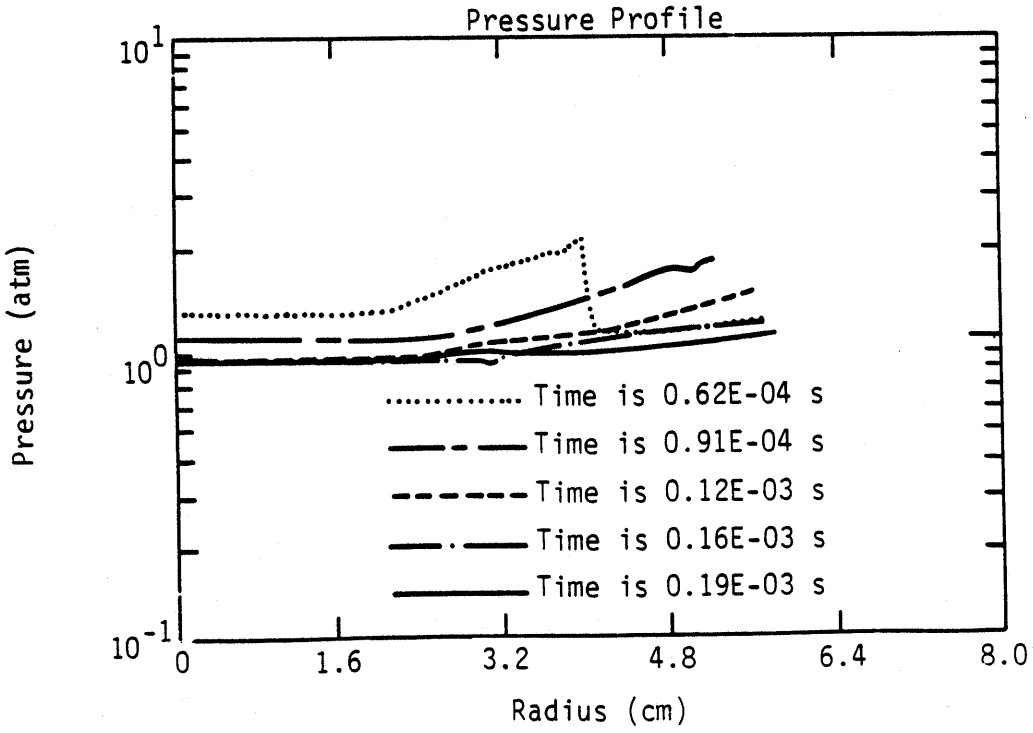

Figure 5. Pressure profiles as the shock wave passes through the transmitting grid boundary.

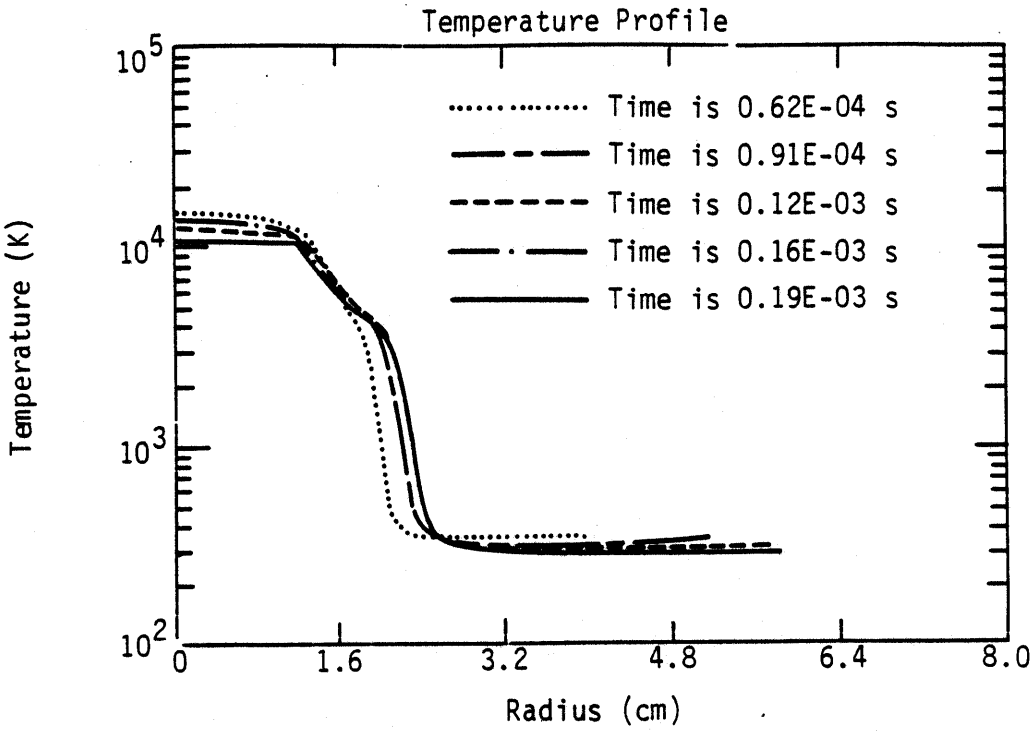

Figure 6. Temperature profiles of a lightning channel.

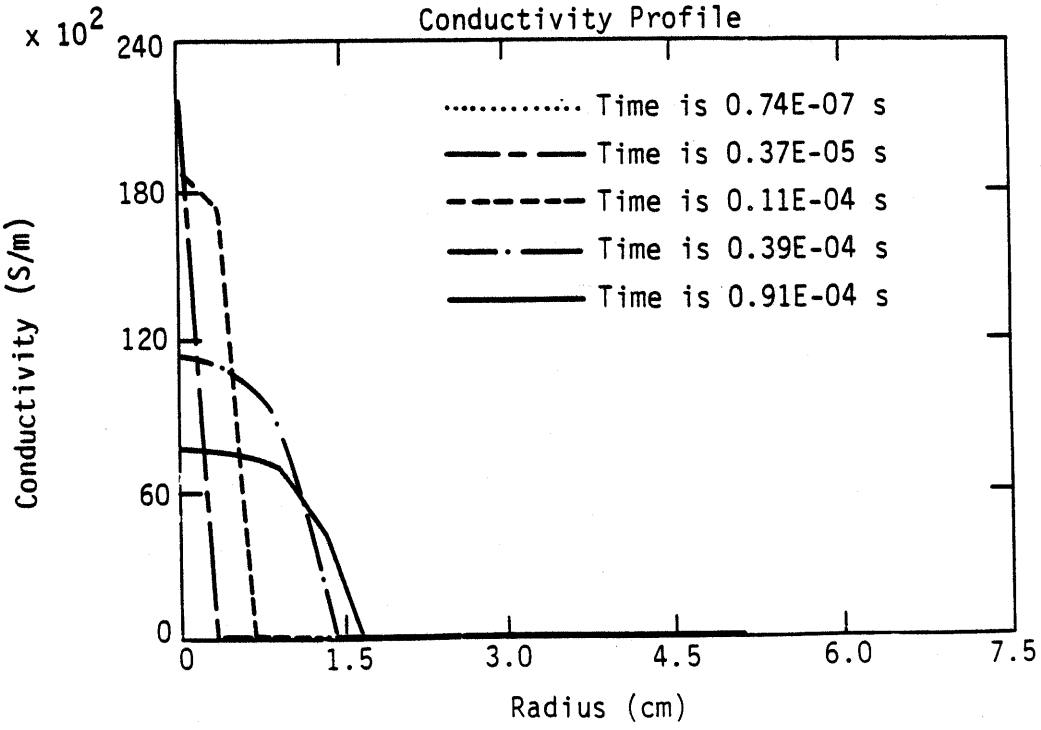

Figure 7. Conductivity profiles of a lightning channel.

The temperature behind the shock wave is slightly above the ambient temperature, however.

Electrical conductivity profiles are shown in Figure 7. The curves are similar to the temperature curves but experience a sharp cutoff between 6,000 and 8,000 K, depending on the density. The conductivity increases rapidly with temperature between 8,000 and 15,000 K, but is fairly flat above 20,000 K. (See Ref. 8, Fig. 1.)

Simulated spectral temperatures are plotted as a function of time in Figure 8. Our temperature curve peaks at a lower value than Plooster's[2] and decreases more rapidly.

The energy balance for our natural lightning simulation is shown in Figure 9. By the time 64 μs have passed (not shown on Fig. 9), 97 percent of the total energy input has been reached. The peak internal energy occurs at this time. About 69 percent of the energy input has been radiated away, while 29 percent of it has gone into an internal energy increase of the gas and 2 percent of it has been converted to kinetic energy. Values read from Reference 2, Figure 6 are also plotted on our Figure 9. Our energy input is higher than Plooster's with about the same energy put into internal energy, while our radiation losses are significantly larger than his. Plooster's values of kinetic energy were not plotted because they are essentially the same as ours.

It is also of interest to compare our model with experimental data for the light output from natural lightning. Guo and Krider have estimated the peak radiance per unit length of natural lightning channels from experimental measurements of the optical power intercepted by a detector as

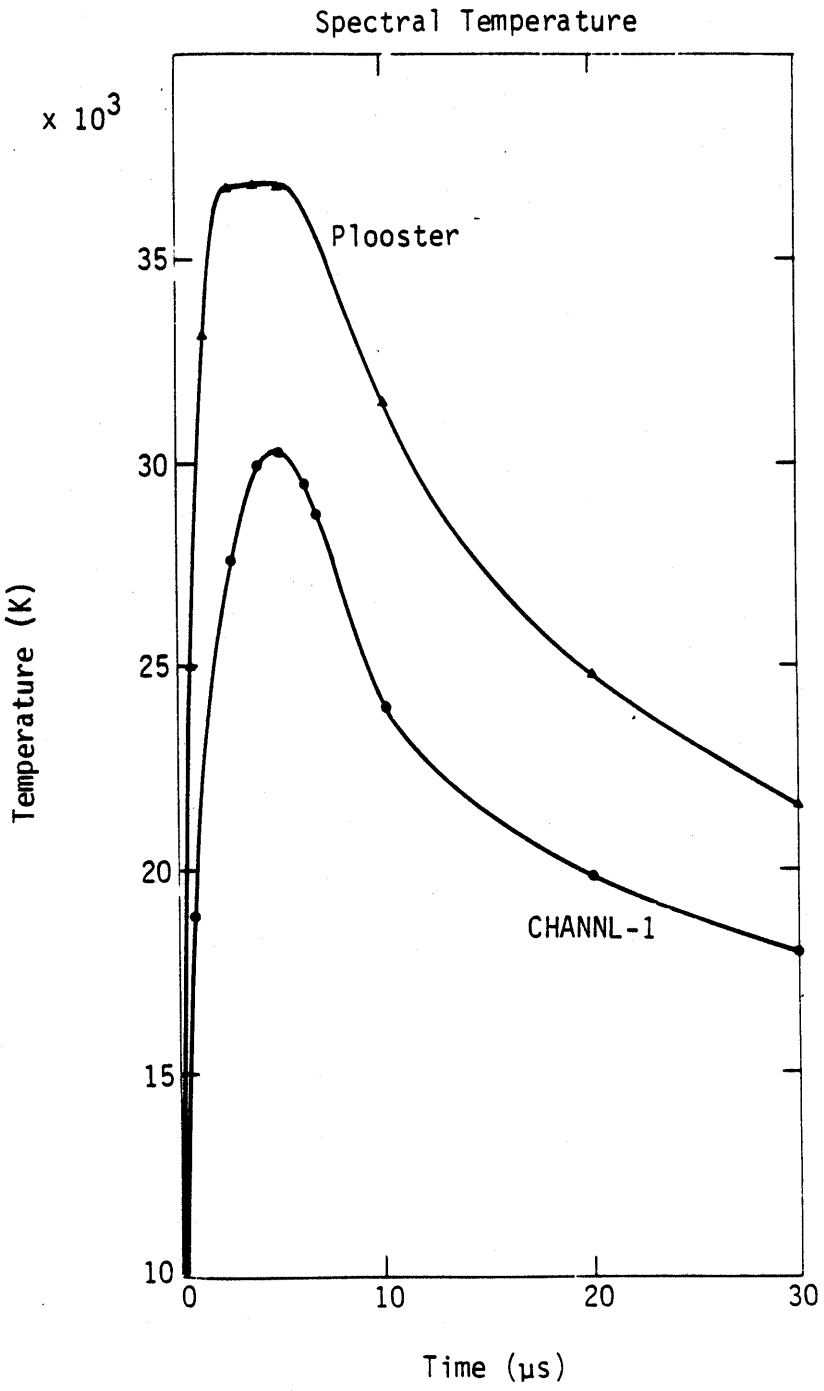

Figure 8. Simulated spectral temperature calculated from the intensity ratio of two N_{II} lines. This ion temperature is almost the same as the temperature at the center of the channel. Results of calculations by Plooster[2] are also shown.

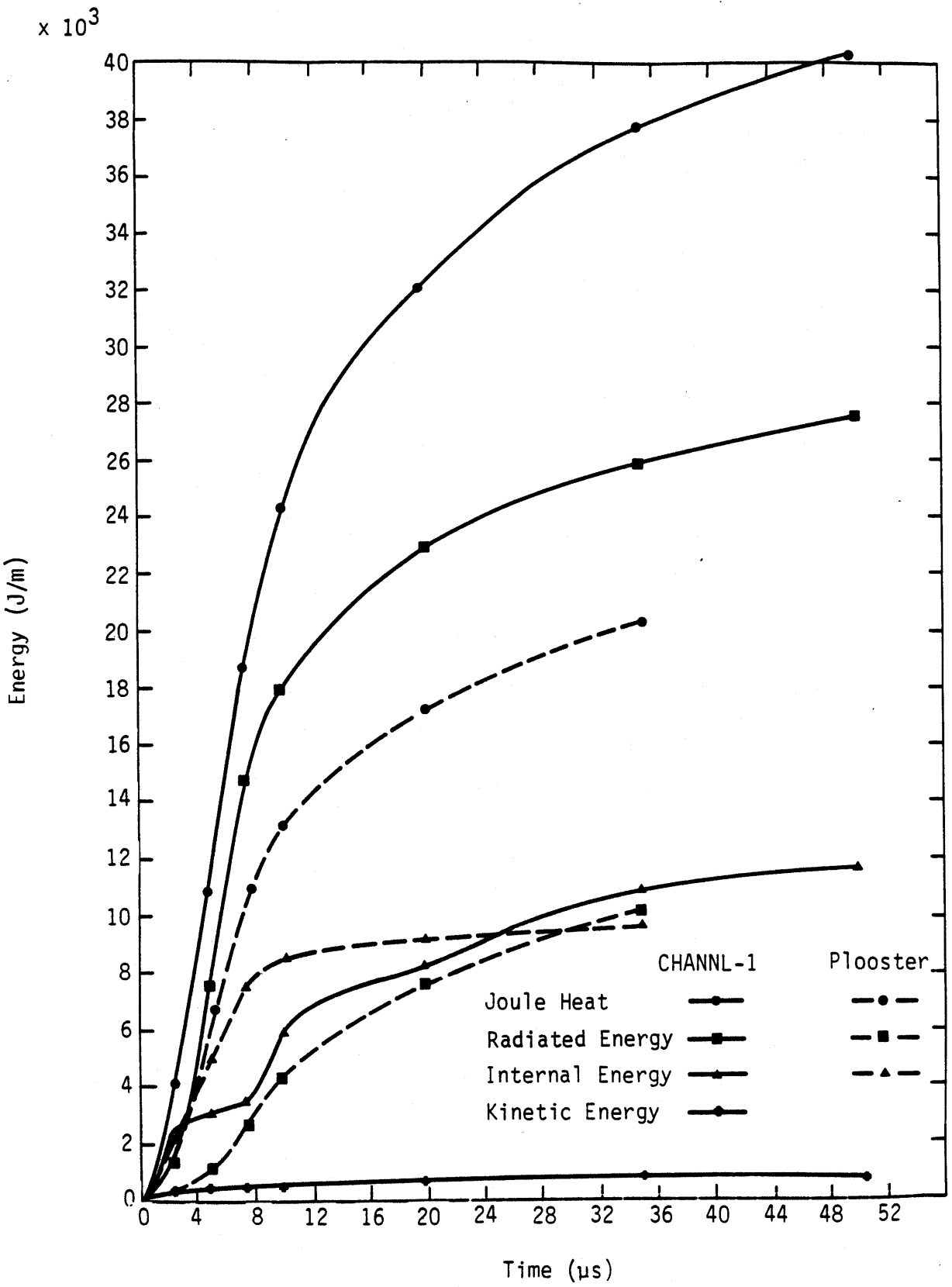

Figure 9. Energy balance for a 20 kA lightning return stroke.

a function of time.[1] To obtain the estimates, they assumed: (1) a straight upward propagation of the luminous front of the return stroke, (2) a constant velocity of propagation, and (3) a constant radiance behind the front. They obtained the equation

$$\frac{dL}{dt} = \frac{\ell_0 v}{4\pi R^2} \tag{33}$$

where L is the detected light signal, ℓ_0 is the initial radiance per unit length of the channel, v is the return stroke velocity, and R is the horizontal distance to the lightning. Their distribution of the initial radiance per unit length is shown in Figure 10, which is taken from Reference 1. They reported a mean initial radiance per unit length for first strokes as $1 \pm 0.9 \times 10^6$ W/m. The nature of these approximations makes this value a lower limit for the actual value. Guo and Krider also recorded the electric field values resulting from the lightning strokes. An approximate equation relating the initial electric field to the initial current has been given by Uman [17]

$$E(t) = \frac{\mu_0}{2\pi} \frac{vI(t - R/c)}{R} \tag{34}$$

The initial electric fields of two initial strokes described in Reference 1 were about 100 and 170 V/m at distances of R = 13 km and R = 14 km, respectively. Using an average value of 8×10^7 for the return stroke velocity, we obtain values for I of 8 kA and 14 kA. These values are uncertain by at least -50 percent, +100 percent due to the variation in return stroke velocities, which were not measured for these cases. The validity and limitations of Eq. 34 are discussed in Ref. 18.

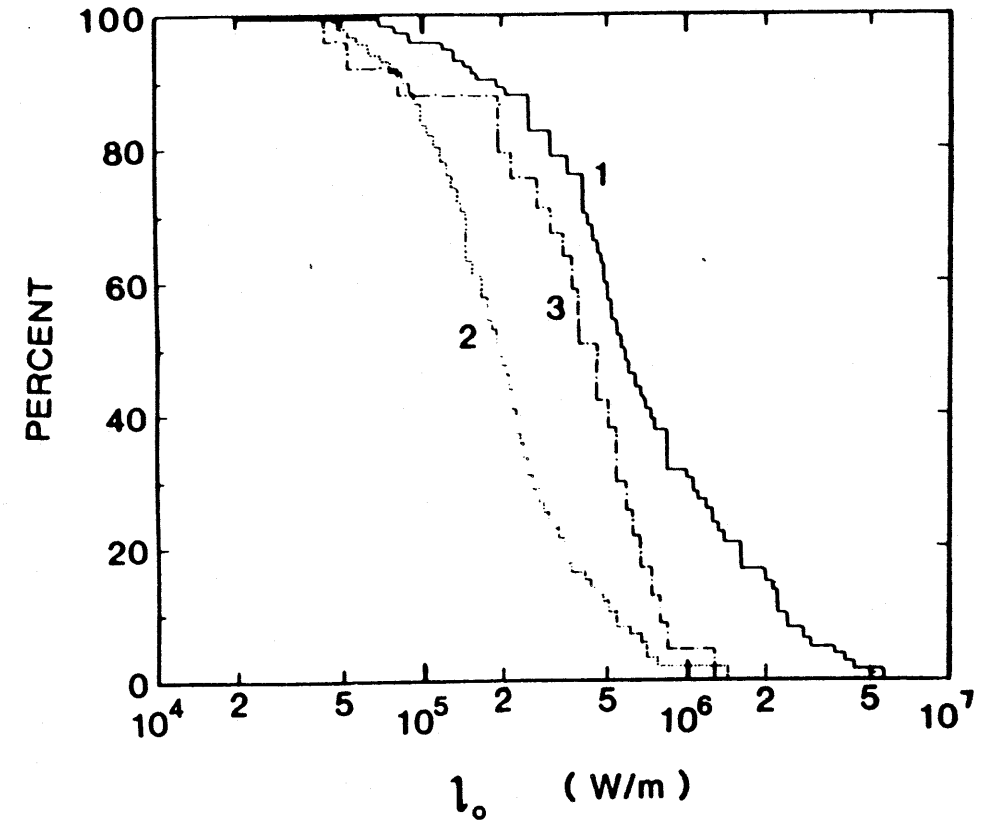

Figure 10. Cumulative distribution of ℓ_0, the initial average channel radiance per unit length. Curve 1 is for first return strokes, curve 2 is for normal strokes. Taken from Guo and Krider, Reference 1.

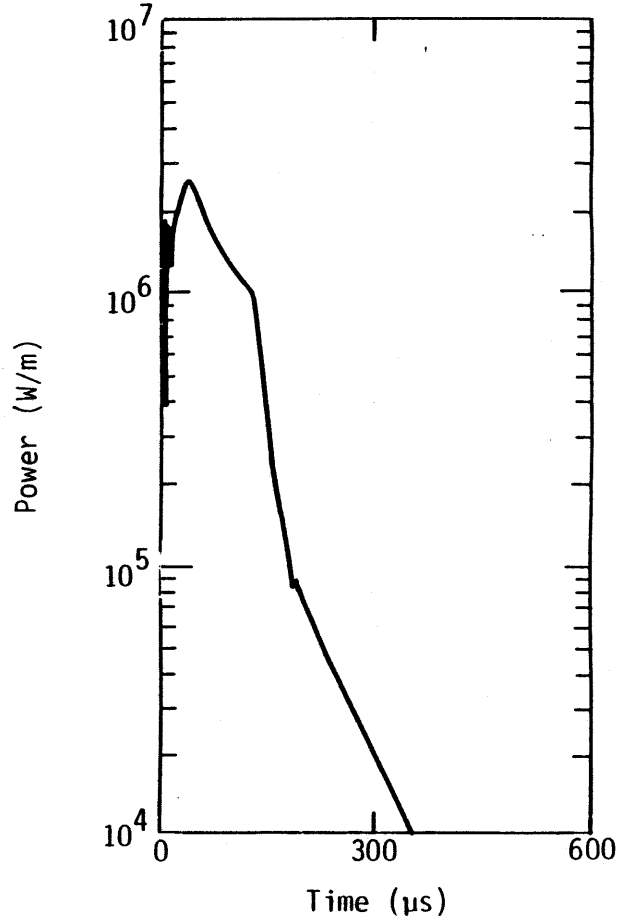

Figure 11. Optical radiance per unit length predicted for a 20 kA lightning return stroke channel.

The calculated values of the radiance versus time of the channel in the 0.4 μ to 1.2 μ wavelength band for a 20 kA pulse are shown in Figure 11. The detector used by Guo and Krider had a spectral response curve that matched this band quite well. Our peak radiance is about 2.5×10^6 W/m, which is in very good agreement with the measurements of Guo and Krider.

REFERENCES

1. Guo, Changming and E. Philip Krider, J. Geophys. Res., 87 8913 (1982).

2. Plooster, M. N., Phys. Fluids 14, 2124, (1971).

3. Baum, C. E., "Properties of Lightning Leader Pulses", Lightning Phenomenology Notes, Note 2 EMP Series, Kirtland AFB, NM 87117.

4. Baum, C. E., and L. Baker, "Return-Stroke Transmission Line Model", Lightning Phenomenology Notes, Note 13, EMP Note Series, Kirtland AFB, NM 87117, 1984.

5. Gardner, R. L., A Model of the Lightning Return Stroke, Ph.D. Thesis, University of Colorado, Boulder, CO, 1980.

6. Plooster, M. N., "Shock Waves from Line Sources" NCAR TN-37, National Center for Atmospheric Research, November 1968.

7. Plooster, M. N., Phys. Fluids 13, 2665 (1970).

8. Plooster, M. N., Phys. Fluids 14, 2111 (1971).

9. Richtmeyer, R. D., and K. W. Morton, Difference Methods for Initial Value Problems, Interscience Publishers, New York, NY, 1967.

10. Finkelnburg, W., and H. Maecker, "Elektrische Bogen and thermisches Plasma" in Handbuch der Physik, edited by S. Flugge, Springer-Verlag, Berlin, Vol. 22, 1956.

11. Spitzer, L., Jr., and R. Harm, Phys. Rev., 89, 977 (1953).

12. Olsen, H. N., Phys. Fluids, 2, 614 (1959).

13. Baker, Louis, CHARTB Multigroup Transport Package, SAND-79-0386, Sandia National Laboratories, Albuquerque, NM, March 1979.

14. Johnston, R. R., R. K. M. Landshoff, and O. R. Platas, Radiative Properties of High Temperature Air, LMSC D267205, Lockheed Palo Alto Research Laboratory, Palo Alto, CA, 15 April 1972.

15. Johnston, R. R., and D. E. Stevenson, Radiative Properties of High Temperature Air, II SAI-056-77-PA, Science Applications, Inc., Palo Alto, CA.

16. Picone, J. M.,J.P. Boris, J.R. Greig, M. Raleigh, and R.F. Fernsler, J. Atmos, Sci., 38 2056 (1981).

17. Uman, M. A., McLain, D. K., and E. P. Krider, Am. J. Phys., 42, pp. 33-38, (1975).

18. Gardner, R. L., C. E. Baum, L. Baker, D. J. Andersh, and J. L. Gilbert, "Comparison of Lightning and High Altitude Electromagnetic Pulse as Potential Threats to Aircraft," Lightning Phenomenology Notes, Note 12, EMP Note Series, Kirtland AFB, NM, 87117, 1984.